A parametric study of FRP Plate Debonding Using Global Energy Balance

Guan G.X., Burgoyne C.J. & Achintha M.

Abstract

Fiber reinforced polymer (FRP) plate debonding is commonly caused by the fracturing of concrete but there have been few studies of fracture debonding models from which the failure load of the concrete cover layer can be evaluated. This paper presents a parametric study for plate end debonding using the global energy balance approach (GEBA), which has recently been proposed for determining structure debonding load. GEBA determines the debonding load using moment-curvature (M-κ) models, and can thus be used to determine how debonding is affected by the beam's flexural design. This paper presents parametric results using debonding contours on plots of moment capacity against the plate curtailment locations, and shows that beams with the same depth-to-fracture-energy ratio give virtually the same debonding contour. This helps to generalise debonding determination for beams with different depths, and can be conveniently used for design. The parametric study lays a foundation to the application of fracture mechanics in FRP plate retrofitting design using conventional M-κ models to cover a wide range of flexural retrofitting situations.

Keywords

FRP; Plate end debonding; Energy release rate; Fracture energy; Global energy balance approach; Debonding contour.

---

[1]**Garfield X. Guan** is an engineering consultant active in Hong Kong and China industry with special focus on value engineering. He received his BEng degree in civil engineering from the University of Hong Kong and his

PhD from University of Cambridge. His research interests include RC structure retrofitting, concrete fracture mechanics and seismic engineering. Garfieldkwan@gmail.com

[2]**Chris J. Burgoyne**: is reader in concrete structures and head of the Structures Group at the University of Cambridge. He has been involved in studies of the application of high strength fibres and advanced composites to structural engineering problems for many years. Corresponding author: cjb@eng.cam.ac.uk

[3]**Mithila Achintha**: is a lecturer in Structural Engineering, Dept. of Engineering and the Environment, University of Southhampton, Mithila.Achintha@soton.ac.uk

Introduction

The debonding mechanism can take two forms; either by debonding at the plate end (PE debonding), or from a location within the beam from an intermediate crack (IC debonding). IC debonding is more complex since the debonded FRP plate can still take loads. IC debonding normally occurs at high loads (Achintha and Burgoyne 2011), whereas PE debonding often takes place at lower loads. This paper addresses only the PE debonding problem.

PE debonding has been recognised as a common failure mechanism in FRP-plate retrofitted beams. The FRP strengthening industry can successfully prevent adhesive layer failure or concrete-adhesive interface failure by correct choice of adhesive and the use of careful surface preparation and curing techniques (Burgoyne et al. 2012). The most likely PE debonding mechanisms are now cover rip-off (Burgoyne et al. 2012; Smith and Teng 2002; Buyukozturk et al. 2004; Aprile et al. 2001), where a relatively thick layer of concrete breaks off while remaining attached to the FRP plate or debonding in the concrete close to the interface. In both cases debonding is inherently the fracture of concrete; many detailed fracture studies have been carried out focusing on the PE debonding region (Hamoush and Ahmad 1990; Davalos et al. 2006; Taljsten 1997; Wu et al 2010; Yang et al. 2003), but the relationship between these local fracture-related properties and the beam structural capacity is still not well understood.

The Global Energy Balance Approach (GEBA) has been proposed to compare the rate at which energy is released (G_R) from the beam with the energy needed to make the fracture propagate (G_f) using moment-curvature (M-κ) models. At first a modified Branson-type M-κ model which treats the FRP plate and the RC section as separate layers was used to describe

the behaviour of the plated RC beam and thus to determine G_R (Achintha and Burgoyne 2008, 2009). Then the FRP-plated RC section was found able to be taken as a whole section when determining G_R using the M-κ model proposed in Guan and Burgoyne (2014a), which enables a relatively easy parametric study to carry out, and thus this paper. A number of factors involved in the section analysis for M-κ model formulation such as steel ratio can affect G_R, thus in order to make the GEBA method more accessible to design, it is desirable to carry out a parametric study to show how the various factors are inter-related.

A parametric study is carried out here with the GEBA using the whole-section M-κ model M1 proposed in (Guan and Burgoyne 2014a) for PE debonding. It allows the investigation of the significance of the various design parameters, and makes GEBA available for design. The full analysis considers many variables (such as the amount of steel, FRP plate, and concrete strength) but for a parametric study to be useful, it is necessary to group the various elements together by the introduction of a number of non-dimensional parameters. However, it is by no means clear what those parameters should be, so this aspect is considered first.

Debonding evaluation using fracture mechanics

Review of global energy balance approach (GEBA)

In view of the overall energy for the plated RC beam under loads, the basic concept of GEBA outlined in Achintha and Burgoyne (2008), and Guan and Burgoyne (2014a) can be described as follows: When a reinforced concrete beam that has been retrofitted with a FRP plate (FRP-RC) is bent, the external load causes associated flexural and shear cracks, and may propagate debonding fractures in the concrete cover layer. The additional work done by the load goes mainly into the change in energy of beam bending, but also possibly into fracture energy relating to the newly formed debonding crack (Eq. 1).

$$W_{ext} = \Delta E_{\text{beam}} + \Delta E_{\text{fracture}} \quad (1)$$

Thus, the energy that is available for release ($\Delta E_{\text{fracture}}$) when the debonding fracture propagates can be obtained from the difference of the additional external work done and the change in beam energy during debonding propagation. Since debonding is a sudden event, the objective is to find $\Delta E_{\text{fracture}}$ at given loads.

One FRP-RC beam can be taken as an integration of a number of beam sections along its span. M-κ relationship is used to determine the energy state of each section, where the section moment can be obtained from the bending moment diagram under the external load. A integration details from section to global quantity can be found in Guan & Burgoyne 2014a. In those parts of a statically determinate beam remote from the debonding location, the moment and curvature do not change when fracture occurs. In the area around the plate end, shown as the 'transfer zone' in Fig. 1 (a), the stresses *do* change. In the transfer zone the force in the FRP is building up from zero to the value it would have if it were fully-bonded to the concrete when the strains of the FRP plate and concrete are compatible. The transfer zone, where the FRP plate is partially-bonded to the concrete and the strains are not compatible, was taken by Achintha & Burgoyne (2008) to extend for about 30 times the plate thickness.

Figure 1 (b) shows a schematic M-κ relationship for a given section in the transfer zone (Section A). In PE debonding, the section will be close to the plate end and the steel will not be yielding, and therefore the nonlinearity of the concrete response is usually insignificant.

Curve (i) shows the expected behaviour of section A before debonding has occurred. The loading curve OEP is kinked because the section is initially uncracked, but then loses stiffness. The line PO represents the assumed unloading curve and the area OPD represents the elastic strain energy of the section. If debonding occurs such that the moment remains constant (as will happen with a statically determinate beam), additional curvature takes place, altering the section M-κ state from P to Q. The line OFQ is notional but represents the section response that would have been expected from initial loading if the debonding had occurred before any loading took place (as in the lower image in Fig 1(a)). QO is the unloading line after debonding has occurred, and the area OQC gives the corresponding section strain energy.

The areas OEPO and OFQO are the energy that is dissipated in forming flexural cracks in the two different states. Since these should not be affected by the amount of debonding that has occurred, it is assumed in this analysis that the two areas are the same. As a result, the additional energy stored in the beam section (ΔE^{A}_{Beam}) during debonding is equal to the change in the section strain energy ΔE^{A}_{Strain}, given by the area of OQCO minus the area of OPDO, which is equal to the area of OPQO (Eq. 2).

$$\Delta E^{A}_{Strain} = \frac{1}{2} M^{A}_{ext} (\kappa^{A}_{Q} - \kappa^{A}_{P}) = \frac{1}{2} M^{A\,2}_{ext} \left(\frac{1}{B^{A}_{Q}} - \frac{1}{B^{A}_{P}} \right) \quad (2)$$

where M^{A}_{ext} is the external moment of section A; κ^{A}_{P} and κ^{A}_{Q} are the section curvatures before and after debonding respectively; while B^{A}_{P} and B^{A}_{Q} are the corresponding effective bending stiffnesses.

The area PQDC is the additional work done (W_{ext}^{A}) by the external section moment during debonding. If a debonding crack extends by a length *a* in the process, the energy release rate (G_R) is given by Eq.3:

$$G_R = \frac{W_{ext} - \Delta E_{strain}}{ba} \tag{3}$$

where *b* is the width of the debonding crack, and W_{ext} and ΔE_{strain} are the overall external work done and the total strain energy in all sections in the transfer zone. This energy is available to form new fracture surfaces. If more energy is released than is needed to form new fractures, the structure will debond suddenly.

Since the FRP plate in the transfer zone is partially-bonded, its strain differs from that in the adjacent RC section. If the effect of the partially-bonded FRP plate can be included in the determination of the M-κ relationship, (Points P and Q in Fig. 1(b)), its effect on the section energy would already have been included in the strain energy calculation.

The energy that can be released to propagate a debonding fracture is the energy that could be recovered in an unloading process. However, unlike the situation for M-κ models in describing the *loading* response, there has been a lack of attention paid to the beam *unloading* response. The assumption here assumes linear-elasticity so that beam sections close to the plate ends would unload to the origin (Fig.1 (b)). Since the external moments are smaller at the plate end vicinity compared to those at midspan, the steel at the plate end vicinity would not yield in *premature* PE debonding. Thus linear-elasticity would be the case in an ideal test

where no debris fell into cracks preventing deformation recovery in PE debonding consideration here. However, if the steel were yielding in the area where the plate is debonding a revised analysis would be required, which may happen in IC debonding (Achintha and Burgoyne, 2008).

In previous GEBA work, Achintha & Burgoyne (2008, 2009) calculated the section strain energy by considering the FRP plate and the RC section as separate elements, and considering the force in the FRP as a prestress on the RC section. The total energy of an FRP-RC section is then the sum of three components as the energy in the FRP plate, the flexural energy in the concrete section, and the energy corresponding to the axial effect of the FRP plate on the concrete section. This energy component treatment needs a reference axis to separate the FRP effect from the concrete response, and results in a more complicated energy description (Achintha and Burgoyne 2008, 2009). The simpler approach, considering the whole FRP-RC section, has been validated against test results and compared with Achintha & Burgoyne's separate section model (Guan and Burgoyne 2014a). Fig. 2 shows one such comparison between the two kinds of models for for Beam A4 in (Arduini et al. 1997).

The curves show the relationship between G_R and the curtailment location when the beam is under its recorded peak load. Both models predict a curtailment slightly greater than the real curtailment, i.e. plate end location, but the predictions are within one concrete cover thickness variation. The trends of both models are similar and the variation in predictions is small. More detailed comparison can be found in Guan and Burgoyne (2014a). Thus it is accurate to use the whole-section models, and its use allows a simpler strain energy computation, which opens the way to a parametric study of debonding.

The M-κ relationship of a section is affected by the force in the FRP plate, thus altering the value of G_R, so the FRP force in the transfer section needs to be determined. The real FRP force ($F_{p\text{-}RL}$) there is lower than it would be if the FRP were fully-bonded ($F_{p\text{-}FB}$), and varies over a distance of $30t_f$ from the effective end of the plate exponentially, as shown in Fig. 3 (Achintha and Burgoyne 2008). The exponential coefficient λ depends on the adhesive properties and a proposed expression in Athintha and Burgoyne (2008) is used, given by $\lambda = \sqrt{G_a /(t_a E_f t_f)}$, where G_a, and E_f, are the shear and elastic modulus of the adhesive and the FRP plate; t_a and t_f are the thickness of the adhesive and the FRP plate.

In a GEBA analysis, a section is first analysed assuming that the FRP is fully-bonded, so plane sections remain plane, giving $F_{p\text{-}FB}$, which is then used to determine $F_{p\text{-}RL}$, and then the section is analysed again using the real FRP force to obtain the energy release rate.

Whole-section moment-curvature model

A number of M-κ models have been proposed that can be applied to the complete FRP-RC section for GEBA use, and these have been compared in Guan and Burgoyne (2014a). The best of the whole-section treatments (the M1 model) is used for the parametric study here and is described briefly. A typical strain profile and forces for uncracked (concrete fully effective in tension) and fully-cracked (concrete carries no tension) sections are shown in Fig. 4. In this figure, F_{cc} , F_{ct} , F_{sc} , F_{st} , F_p are the resultant forces of concrete in compression, concrete in tension, compression steel, tension steel, and FRP retrofitting plate respectively; ε_s , ε_{sp} , ε_f , ε_1 , ε_2 are the strains at tension steel, compression steel, FRP plate, and the top and bottom concrete fibre respectively; y is the distance from the neutral axis to the F_{sc}.

The principles behind the M1 section analysis are outlined in Fig. 5 (Guan and Burgoyne 2014a): the cracking (κ_{cr}, M_{cr}) and yielding (κ_y, M_y) states are first calculated so the section can be classified as uncracked ($M_{ext} \le M_{cr}$), partially-cracked ($M_{cr} < M_{ext} < M_y$) or fully-cracked ($M_{ext} \ge M_y$); the appropriate technique can then be used to analyse the section. For an uncracked or fully-cracked section, the analysis is straightforward and the effective stiffness (B) is calculated as:

uncracked and fully-cracked sections: $$B = M_{ext} / \kappa \qquad (4)$$

When a section is partially-cracked, two separate analyses are carried out (1) as if it were uncracked and (2) as if it were fully-cracked. This gives the points (κ_{uc}, M_{ext}) and (κ_{fc}, M_{ext}) in Fig. 5. The stiffness is interpolated to obtain the exact M-κ state (the 'triangle' in Fig.4):

$$B_{pc} = K_p B_{uc} + (1 - K_p) B_{fc} \qquad (5)$$

where $$K_p = \left(\frac{M_{cr}}{M_{ext}} \right)^4 \left(1 - \left(\frac{M_{ext} - M_{cr}}{M_y - M_{cr}} \right)^4 \right)$$

B_{uc} and B_{fc} correspond to the curvature obtained from solving the partially-cracked sections as if they were uncracked and fully-cracked. K_p is the interpolation coefficient to ensure the M-κ curve is continuous at first-crack (κ_{cr}, M_{cr}) and first-yield (κ_y, M_y) for the whole FRP-RC section, which is modified from the expression used in Achintha & Burgoyne (2009) for RC section.

When the M-κ relationship is obtained, the strain energy and the energy release rate (G_R) can be determined. G_R is then determined following the procedures in Guan & Burgoyne (2014a) for plate end debonding computation, using the M1 model.

Determination of concrete fracture energy

In a debonding analysis based on fracture mechanics, once G_R has been obtained, it is compared with the concrete fracture energy (G_f) to see whether a crack can propagate. G_f associated with FRP-RC beam debonding is rarely assessed in experimental studies, even though FRP debonding is clearly a fracture event. The determination of G_f depends on many microstructural features such as size, shape, surface texture and location of the aggregate pieces, and also on the distribution of voids in the mix. Although there have been various experimental investigations to determine G_f, they were often associated with practical and conceptual difficulties. In PE debonding, a combination of normal and shear stress concentrations will be present in the vicinity of an existing interface crack so the exact G_f should be a complicated mixed-mode fracture energy. Burgoyne et al. (2012) discuss nature and mode mixity of concrete fracture energy and conclude that the Mode I fracture energy should be used. By definition, this is the overall energy required to open a traction-free crack of unit area. Bazant & Becq-Giraudon (2002) reviewed a large number of the previous fracture tests and proposed an empirical expression to determine this value (Eq. 6).

$$G_f = 0.0025\alpha_0\left(\frac{f_c'}{0.051}\right)^{0.46}\left(1+\frac{d_a}{11.27}\right)^{0.22}\left(\frac{w}{c}\right)^{-0.30} \quad \text{in N/mm} \qquad (6)$$

where w/c is the water/cement ratio by weight, d_a is the maximum aggregate diameter, α_0 takes 1 and 1.44 for rounded and crushed aggregates respectively. The G_f value from Eq.4

usually ranges from 0.07 N/mm (for ordinary concrete with 10 mm rounded aggregate) to 0.17 N/mm (for ordinary concrete with 40 mm crushed aggregate). For the parametric study here, G_f is taken as 0.15 N/mm which approximately corresponds to ordinary concrete with 20 mm crushed aggregate.

Parametric study of GEBA

Simplified analysis to determine relevant parameters

The GEBA is relatively complicated and involves many parameters. In order to determine which are the relevant parameters to be used in a parametruc study, a very simplified analysis is presented here to determine the key parameters. The parametric study itslef, which follows is then carried out numerically using the detailed GEBA with the M-κ model M1 (Guan and Burgoyne 2014a).

Energy release rate G_R is computed from the difference between the work done by the external loads and strain energy (Eq.1-3) released during the debonding fracture. Since strain energy is determined from the M-κ relationship, G_R is related to the design of the beam section. For the purpose of deriving the relevant non-dimensional parameters, a typical sectional analysis as used in design is applied: Consider a fully-bonded FRP-RC section at the point of yielding, and without compression steel. The strains in the various materials can be determined by considering equilibrium of the section force (Eq. 7) and moment (Eq. 8) using the symbols shown in Fig. 4:

$$\rho_s b d f_y + \rho_f b d E_f \varepsilon_f = \alpha f_c' b x \tag{7}$$

$$M_{ext} = \rho_s b d f_y (d - x + y) + \rho_f b d E_f \varepsilon_f (d - x + y + c + t_a + t_f / 2) \tag{8}$$

ρ_s (= A_s / bd) and ρ_f (= A_f / bd) are the FRP and steel ratio of a beam section, and α is a numerical coefficient such that $\alpha f_c'$ represents the average concrete compressive stress in the compression zone as is normal in beam design. The moment in Eq.8 is taken about the point of action of the resultant concrete compression force.

Since the section is assumed to be fully-bonded, the geometric relationships in Fig. 4 give

$$\varepsilon_f = \frac{d - x + c + t_a + t_f/2}{d - x}\varepsilon_s = \frac{\left(d - x + c + t_a + t_f/2\right)}{d - x}\left(\frac{f_y}{E_s}\right) \tag{9}$$

In order to deduce to the most important parameters, the concrete cover thickness (c), and the FRP plate and adhesive layer thickness (t_f+t_a) are initially ignored; their influence on debonding is discussed in detail later. Substituting Eq. 9 into Eq. 8 gives

$$M_{ext} \approx bd^2\left(f_y\rho_s + f_y\rho_f\frac{E_f}{E_s}\right)\left(1 - \frac{x}{d} + \frac{y}{d}\right) \tag{10}$$

Eq.10 can be made dimensionless with the conventional flexural design section property ($f_c' bd^2$):

$$\frac{M_{ext}}{f_c' bd^2} \approx \left(\rho_s\frac{f_y}{f_c'} + \rho_f\frac{f_y}{E_s}\frac{E_f}{f_c'}\right)\left(1 - \frac{x}{d} + \frac{y}{d}\right) \tag{11}$$

Eq.11 shows that the non-dimensional moment (section capacity) for an FRP-RC beam is affected by the steel and FRP material ratios ρ_s and ρ_f. The strain energy at the designed section is then:

$$E_{strain} = \frac{M_{ext}^{\ 2}}{2B} = \left(bd^2 \left(\rho_s f_y + \rho_f E_f \frac{f_y}{E_s} \right) \left(1 - \frac{x}{d} + \frac{y}{d} \right) \right)^2 \Big/ 2B \qquad (12)$$

The effective stiffness B of an FRP-RC section comes from the stiffness of different materials (steel bars, FRP plate and concrete) but it can be considered as a composite section with the effect of the various materials included in a single parameter C.

$$2B = CE_c bd^3 \qquad (13)$$

C is the unique stiffness ratio coefficient depending on the section design and E_c is the concrete elastic modulus

Substituting Eq.13 into Eq.12, gives

$$E_{strain} = \frac{M_{ext}^{\ 2}}{2B} = \frac{1}{E_c C} bd \left(\rho_s f_y + \rho_f E_f \frac{f_y}{E_s} \right)^2 \left(1 - \frac{x}{d} + \frac{y}{d} \right)^2 \qquad (14)$$

Eq.13 gives the strain energy in a unit length of the beam, which is affected by the amount of steel and FRP material. As with Eq.10, Eq.14 can be made dimensionless by $f_c' bd$, and denoted as Ω here:

$$\Omega = \frac{E_{strain}}{f_c' bd} = \frac{M_{ext}^{\ 2}}{2B} = \frac{1}{C} \frac{f_c'}{E_c} \left(\rho_s \frac{f_y}{f_c'} + \rho_f \frac{f_y}{E_s} \frac{E_f}{f_c'} \right)^2 \left(1 - \frac{x}{d} + \frac{y}{d} \right)^2 \qquad (15)$$

335

336 Thus the non-dimensional energy term Ω , is also dependent on the steel and FRP material
337 ratios, ρ_s and ρ_f, in the same way as the non-dimensional moment. However, the energy
338 release rate G_R , which is related to E_{strain} / b , has dimensions, and its value is affected by the
339 section size. E_{strain} represents the energy stored per unit length of the beam, and varies over
340 the length of the transfer zone, which is taken as fixed ($30t_f$)(Achintha and Burgoyne, 2008).
341 The more strain energy that is stored in the transfer zone, the more that is available to be
342 released. Thus the G_R is reflected in E_{strain}/b and is largely determined by the term $f_c'd\Omega$.
343 Since $f_c'd\Omega$ is proportional to d, then G_R should be proportional to d.
344

345 If the material properties of concrete, steel and FRP plate are fixed, it is noted from the
346 dimensionless part of $f_c'd\Omega$ (i.e. Ω), that G_R for a particular load distribution depends on the
347 tension steel ratio (ρ_s), the FRP ratio (ρ_f) and the Young's moduli. Thus the tension steel
348 ratio and FRP ratio are important parameters. In the dimensioned part, the effective beam
349 depth (d) is the key parameter. Additionally, although compression steel does not affect
350 Eq.15 due to the simplification in derivation, it is almost invariably present in a beam and
351 therefore the effect of compression steel ratio (ρ_{sp}) is also studied. Furthermore, due to the
352 simplified approximation from Eq.8 to Eq.12, there is no term relating to the concrete cover
353 thickness, but it always exists in RC beams. Hence its influence on G_R is also examined in the
354 non-dimensional form c/d.
355

356 When considering material properties, the concrete compressive strength is usually within the
357 range of 30 to 60 MPa. For the FRP, which never reaches its failure strain and behaves
358 elastically, the effect of its elastic modulus should be similar to the effect of its amount (ρ_f),

and therefore the elastic modulus effect is not discussed. The effect of all these parameters is presented later.

Construction of the parametric space

Since the bending moment changes with the load and the location, both the change of mid-span external moment (which affects the design of the cross-section) and the curtailment location affect the value of G_R (Athintha and Burgoyne 2011; Guan and Burgoyne 2014a). The loading state and the section design vary for every beam, so it is desirable to determine the appropriate factors so that the behaviour of many different beams can be covered in the same chart.

In conventional RC beam design and FRP plate retrofitting design, flexural capacity is usually the primary design target, which is represented by the dimensionless parameter $M/(f_c'bd^2)$, where M is the maximum moment (usually at midspan). Conventional RC beams typically have $M/(f_c'bd^2)$ in the range 0.05 to 0.29 in the most heavily loaded section (Park and Paulay 1975); strengthened beams may be stronger so the range is extended up to 0.4. This parameter is for the section under maximum loading, which controls the amount of FRP that the designer wants to add. The principal decision that has to be taken is where to curtail the plate; this is typically expressed as a fraction of the shear span, (L_{cur}/L_{shear}), where L_{cur} is measured from the support to the plate end.

Using GEBA, as set out in Burgoyne et al (2012), it is now possible to produce a three-dimensional plot showing the variation of G_R with the maximum moment and the curtailment

location for a typical beam (Fig. 6). The result is a curved surface that gets higher as both L_{cur}/L_{shear} and $M/(f_c'bd^2)$ increase. The value of G_f, which is a material property.

The intersection line between the curved G_R surface and the G_f plane indicates when debonding would occur and will be termed the debonding contour (DBC). This can be plotted on a 2D plot of normalized curtailment (L_{cur}/L_{shear}) against normalized loading state ($M/(f_c'bd^2)$) for the midspan section, which can be used to demonstrate the effects of changing the various parameters.

The flexural capacity of the midspan section is not considered as a separate constraint, although in practice it will limit how far the DBC will extend.

Design of the standard beam

For the purposes of comparison, a basic standard beam is considered in Fig. 7, with the properties given in Table 1.

Under each load, G_R is computed for the curtailment length (L_{cur}) varying from 200mm to 600mm. The reinforcing steels is specified as a ratio rather than as a number of discrete bars. The nominal FRP and adhesive layer thicknesses are only used to determine the moment arm when considering the flexural contribution of FRP force in the section. A G_f value of 0.15N/mm is used.

The parametric study is then carried out by changing one variable at a time from the standard beam. The GEBA method, using the whole-section M-κ model M1 in Guan & Burgoyne (2014a) is used to investigate the effects on debonding, and the results are presented below.

Effect of the tension steel ratio

Figure 8 shows the effect on the DBC of varying the tension steel ratio (ρ_s) in the range 0.6% to 2.0% with a step of 0.2%. The moment in the x-axis is the midspan (largest) moment.

The region to the bottom-left of the DBC is the safe zone where G_R is smaller than G_f whilst the region to the top-right of DBC indicates debonding. Curves to the top right of the plot (such as the ρ_s=2.0% line here) show that the section is more resistant to debonding than curves to the bottom left (such as the ρ_s=0.6% line).

It can be concluded from Fig. 8 that: (i) Debonding is less likely to occur with an increasing amount of tension steel, because that steel enhances the section stiffness, resulting in lower curvatures so there is less strain energy available for release. As a result G_R is smaller and the FRP-RC beam is less likely to debond. (ii) The shift of DBC position is relatively even as ρ_s changes, because the tension steel is always fully-bonded within the RC section and its flexural strengthening effect transfers directly into the section without loss.

Effect of the FRP strengthening material ratio

By varying only the FRP ratio (ρ_f) in the standard beam from 0.1% to 1.5% with a step of 0.2%, the changes of the DBC position are as shown in Fig. 9.

Figure 9 is significantly different from Fig. 8 in two respects. (i) Debonding occurs more easily with more FRP material, because a greater ρ_f means more energy is stored in the FRP prior to debonding, all of which is released when fracture occurs. (ii) The change in the DBC

position is small when ρ_f is large (0.7% to 1.5%), while it moves dramatically when ρ_f is small (0.7% to 0.1%). This rapid change is due to the change in the cracking state of relevant beam sections; when ρ_f = 0.7 the sections much less likely to be cracked, while when ρ_f = 0.1% cracking will almost certainly be present. Unlike the tension steel, the FRP plate at the plate end is not fully-bonded and thus its flexural contribution cannot be completely integrated into the section. (iii) Sections with only a small amount of FRP has little risk of debonding because the FRP plate attracts a relatively small load, which limits the amount of energy that can be released.

Figures 8 and 9 show that changing the amount of steel and FRP have opposite effects on the likelihood of debonding. Generally, a beam with a high ratio of ρ_f / ρ_s has to transmit a higher proportion of the tensile force through the bonded region, which will thus make debonding more likely, whereas a lower value makes it less likely. Thus, changing ρ_f and ρ_s have opposite effects. Since both ρ_f and ρ_s are also important parameters in beam strength, the method of selecting optimised ρ_f and ρ_s values should be determined from both the debonding and beam strength consideration, which is beyond the scope of this paper. The details of an FRP retrofitting design method based on the same principles can be found in Guan & Burgoyne (2014b), where the importance of treating steel and FRP ratio is pointed out and the design based on fracture mechanics is explained in a systematic way.

Effect of the compression steel ratio

By varying only the compression steel ratio (ρ_{sp}) in the standard beam from 0 to 1.0% with a step of 0.2%, the changes of the DBC position is as shown in Fig. 10.

It is observed that: (i) the compression steel ratio has little effect on debonding. Furthermore, since the amount of compression steel used is small in practice (<< 1.0%), it can be neglected in debonding consideration, which justifies excluding of compression steel in the derivation of important dimensionless parameters. (ii) Though its effect is limited, increasing the amount of compression steel slightly reduces G_R and makes the FRP-RC beam marginally less likely to debond. The reasoning is similar to the effect of increasing tension steel; more compression steel makes the section stiffer, but because debonding occurs prior to yielding, the strains at the compression steel level are small and the contribution is negligible compared with the adjacent concrete.

Effect of the concrete compressive strength

The effect of varying only the concrete compressive strength of the standard beam is shown in Fig. 11. Since the section does not fail in compression, the principal effect is due to the corresponding change in the tensile strength of concrete. This change affects most significantly the first cracking moment and hence the energy state of a section. Varying the concrete strength will also influence the concrete fracture energy G_f, but this influence is small provided the aggregate type is not altered. Thus, for normal strength concrete G_f is kept constant at 0.15 N/mm when comparing the concrete strength effect.

A beam with higher strength concrete is less likely to debond. A higher concrete compressive strength makes the section stiffer so the curvatures, and hence the strain energy, are lower. It is evident from the figure that when f_c' changes from 30 MPa to 60 MPa, the DBC changes linearly because the concrete remains virtually linear-elastic in the transfer zone..

Effect of the concrete cover thickness

480 The concrete cover influences the section analysis via the geometry, which affects the energy
481 release rate (G_R) computation in GEBA. The concrete cover thickness is studied for standard
482 beams of 400 mm and 800 mm deep. By varying only the cover thickness from 5% to 15% of
483 the beam depth, the change of DBC is as shown in Fig. 12.
484
485 The idealised 'zero cover thickness' condition is also presented to show that in the G_R
486 computation the effect of concrete cover thickness is insignificant. Its influence on energy
487 release rate is small, and that influence is related to the absolute value of the thickness instead
488 of its ratio to the beam depth. Hence it is reasonable not to consider the cover thickness
489 separately in practical design, but to take the beam depth (h) to be the same as the effective
490 beam depth (d).
491
492 It is worth pointing out that GEBA which is based on section analysis assumes the concrete
493 cover layer (commonly within 50 mm thick) is undividable into further sub-layers. It should
494 be noted that a thicker concrete cover layer may lead to higher uncertainty of the safe plate
495 end location (L_{cur}) in a GEBA debonding prediction (Achintha and Burgoyne 2011; Burgoyne
496 et al. 2012). The critical shear crack that develops in the vicinity of the plate end usually
497 propagates at about 45 ºto the interface, up to the level of tension-steel bars in the concrete
498 cover layer (Fig. 13). The peeled part of the plate carries no force, so the effective plate end
499 location ($L_{cur\text{-}e}$) now differs from the actual plate end location (L_{cur}). How far the initial shear
500 crack develops before the critical debonding state occurs determines the location of $L_{cur\text{-}e}$
501 (Athintha and Burgoyne 2011). Take the case in Fig. 12(b) as an example, an uncertain of
502 curtailment ration due to the concrete cover may be up to 120 mm / 1500 mm as 8%, which
503 would then lead to a reduction of debonding load indicated by the corresponding DBC.

Further detailed fracture studies of the concrete cover layer are needed to quantify this uncertainty for GEBA.

Study of the effect of RC section depth

By varying the beam depth only from 200 mm to 1000 mm in the standard beam with a step of 100 mm (keeping the concrete cover as 35mm), the effect of beam depth on DBC is as shown in Fig. 14: debonding becomes easier if the beam depth increases. The contours get closer together as the beam gets deeper.

G_f and beam depth effect on debonding

In order to see if debonding will occur, G_R has to be compared with G_f. It was shown above that G_R is proportional to the effective beam depth d, with a proportional coefficient of dimension of N/mm^2, if the concrete compressive strength (f_c') is fixed. Since, in practice, the concrete cover thickness c is small in comparison to the beam depth h and its effect on DBC is negligible as demonstrated previously, it can also be taken that G_R is proportional to the overall beam depth h.

As a result, the DBC plots can be normalised by using h/G_R instead of G_R for beams that differ only in depth, so a plot of the h/G_R surfaces (similar to Fig. 6) can be envisaged. Beams with different combinations of depth (h) and fracture energy (G_f) are then represented by the same normalised DBC, if they give the same h/G_f value. For instance, if the depth of a reference beam is defined as h_{ref} then it would be expected that for beams of other depths h, their DBCs obtained for an equivalent fracture energy $G_{f\text{-}q}$, where $h/G_{f\text{-}q} = h_{ref}/G_f$ should collapse to a single line. These lines are plotted for a range of beams with depths that vary

528 from 200 mm to 1000 mm in Fig. 15 (taking h_{ref} as 400 mm, G_f as 0.15 N/mm, and $G_{f\text{-}q}$ as
529 $h/h_{ref} \times G_f$,).
530
531 These contours are close to each other as expected. The small discrepancies in the figure
532 come from keeping the concrete cover the same for all the beams with different depths. The
533 DBCs in Fig. 15 are effectively the same as the DBC for the standard beam in the previous
534 figures. Thus each DBC in the previous studies is effectively the DBC for all the beams with
535 the same depth-to-fracture-energy ratio (h/G_f), so there is no need to re-compute the DBC for
536 other beams. This provides a convenient way to consider debonding for beams varying only
537 in depths.
538
539 With other properties the same as the standard beam, the DBCs with various h/G_f values (1.3
540 - 13×10^3 MPa^{-1}) are plotted in Fig. 16, roughly corresponding to the combination of different
541 G_f values ranging from 0.07 to 0.2 N/mm and h changing from 200 to 1000 mm.
542
543 These DBCs have been obtained by cutting the G_R surface of the 400 mm standard beam with
544 horizontal planes at different G_f values. By working instead with h/G_f , instead of computing
545 G_R surfaces for beams with various depths time after time, the G_R surface for the standard
546 beam provides enough information for design use. The designer, knowing the particular
547 value of h and G_f can then find the appropriate h/G_f line in Fig. 16. That figure also shows
548 that there is an important size effect in beams of different depth, and the foregoing analysis
549 shows that this is closely associated with the energy released when the FRP debonds.
550
551 Since $M/(f_c bd^2)$ can be obtained from conventional section calculation, a designer can easily
552 determine the required curtailment from the DBC graph for the beams that differ from the

553 standard beam only in depth. The designer would still need to obtain (or be provided with)
554 one such chart for each combination of beam with other f_c', ρ_s and ρ_f.
555
556 ## Conclusion
557 This paper conducts a fracture-based parametric study for plate end debonding of FRP-RC
558 beams, applying the global energy balance approach (GEBA) based on a modified M-κ
559 model, and has pointed out the significance of different beam section components in
560 debonding consideration.
561
562 It has been shown that plots of the debonding contour (DBC) can be drawn on axes that relate
563 $M/(f_c'bd^2)$ and the curtailment location, with contours of varying tension steel ratio from
564 0.6-2.0%, FRP ratio from 0.1-1.5%, and various concrete compressive strength, in a broad
565 range of normalized loading state ($0.05< M/(f_c'bd^2) <0.4$, at the midspan section). It also
566 considers debonding for beams with different depths, and has found that the energy release
567 rate (G_R) is proportional to the beam depth (h). A normalised debonding criterion which is the
568 DBC at h/G_f (MPa^{-1}) is then proposed to consider the design of beams with different depths
569 (h) and fracture energy (G_f). This normalised contour plot enables the use of only one G_R
570 surface that is computed based on GEBA for a particular beam to represent all the design
571 cases with a certain depth-to-fracture-energy ratio (h/G_f), and therefore it dramatically
572 reduces the number of individual design consideration. Furthermore, all the DBC is plotted
573 against the conventional normalised flexural capacity quantity, which provides a new base to
574 consider debonding prevention and flexural capacity simultaneously in FRP retrofitting
575 design, and should help apply fracture mechanics to practical design. Although this
576 parametric study has considered so far only statically determinate beam situation with no

redistribution of moments and energy, it can be further developed into the regime of indeterminate structures.

Notations

A_s -- Cross-sectional area of tension or compression steel

A_f -- Cross-sectional area of FRP strengthening plate

b -- Width of the RC beam

B -- Overall FRP-RC section stiffness

c -- Concrete cover thickness

d -- Effective depth of the RC beam

E_c -- Young's modulus of concrete

f_y -- Yield stress of tension steel

f_c' -- Concrete cylinder compressive strength

F_{cc} , F_{ct} , F_{sc} , F_{st} , F_p -- Resultant forces of concrete in compression, concrete in tension, compression steel, tension steel, and FRP retrofitting plate respectively

h -- Depth of the RC beam section

L_{cur} -- Curtailment length (the distance from the FRP plate end to the support)

L_{cur} -- Effective curtailment length

L_{shear} -- Shear span of the FRP-RC beam

M_{cr} , M_y , M_{ult} -- First cracking moment, Yielding moment, and Ultimate moment capacity respectively

M_{ext} -- External applied moment

M_{fc} , M_{uc} -- Moment of fully-cracked section and uncracked section respectively

t_f -- Thickness of the FRP strengthening plate

t_a -- Thickness of the adhesive layer

602 W_{ext} -- External work

603 x -- Neutral axis depth from the top RC beam surface

604 y -- Distance between neutral axis and the point of action of the resultant concrete

605 compressive force

606 ε_s , ε_{sp} , ε_f , ε_1 , ε_2 -- Strains at tension steel, compression steel, FRP plate, and the top and

607 bottom concrete fibre respectively

608 ρ_s -- Tension steel ratio (A_s/(bd))

609 ρ_f -- FRP strengthening material ratio (A_f/(bd))

610 κ -- Curvature

611 κ_{cr} , κ_y , κ_{ult} -- Curvature of an RC beam section at first cracking, at first yielding of

612 the tension steel, and at ultimate state respectively

613 κ_{ult} -- Curvature of an RC beam section at ultimate state

614

615 # References

616 Achintha, P.M.M., and Burgoyne, C.J. (2011). “Fracture mechanics of plate debonding:

617 validation against experiment.” Constr. build. Mater. 25: 2961-71.

618 Achintha, P.M.M., and Burgoyne, C.J. (2008). “Fracture mechanics of plate debonding.”

619 J. Compos. Constr. 12(4):396-404.

620 Achintha, P.M.M., and Burgoyne, C.J. (2009). “Moment-curvature and strain energy of

621 beams with external fiber-reinforced polymer reinforcement.” ACI Struct. J. 106(1): 20-9.

622 Aprile, A., Spacone, E., and Limkatanyu, S. (2001). “Role of Bond in RC Beams

623 Strengthened with Steel and FRP Plates.” J. Struct. Eng. 127(12): 1445-52.

624 Arduini, M., Di-Tommaso, A., and Nanni, A. (1997). “Brittle failure in FRP plate and

625 sheet bonded beams.” ACI Struct. J. 94(4): 363-70.

626 Bazant, Z.P., Becq-Giraudon, E. (2002). “Statistical prediction of fracture parameters of
627 concrete and implications for choice of testing standard.” Cem. Concr. Res. 32:529-56.
628 Burgoyne, C.J., Achintha, M., Guan, G.X. (2012). “Prediction of FRP debonding using
629 the global-energy-balance approach.” in ACI SP-286, A Fracture Approach for FRP-
630 Concrete Structures, Edited by Lopez, M. and Carloni, C.
631 Buyukozturk, O., Gunes, O., Karaca, E. (2004). “Progress on understanding debonding
632 problems in reinforced concrete and steel members strengthened with FRP composites.”
633 Constr. Build. Mater. 18(1):1–19.
634 Davalos, J.F., Kodkani, S.S., and Ray, I. (2006). “Fracture mechanics method for model-I
635 fracture evaluation of FRP bonded to concrete substrates.” J. Mater. Civil. Eng. 18(5):
636 732-42.
637 Guan, G.X. and Burgoyne, C.J. (2014a). “Comparison of moment-curvature models for
638 FRP plate end debonding studies using GEBA.” Accepted by ACI Struct. J. (Paper S-
639 2011-280 - in press. Preprint available at http://www-
640 civ.eng.cam.ac.uk/cjb/papers/p81pre.pdf)
641 Guan, G.X. and Burgoyne, C.J. (2014b).” Unified Design Method for Flexure and
642 Debonding in FRP Retrofitted RC Beams.” Accepted by J. Compos. Constr. (in press).
643 Preprint available at http://www-civ.eng.cam.ac.uk/cjb/papers/cp96.pdf
644 Hamoush, S.A., and Ahmad, S.H. (1990). “Debonding of steel plate-strengthened
645 concrete beams.” J. Struct. Eng. 116(2): 356-71.
646 Park, R., and Paulay, T. (1975). Reinforced concrete structures. John Wiley & Sons,
647 Toronto.
648 Smith, S.T., Teng, J.G. (2002). “FRP-strengthened RC beams. I: Review of debonding
649 strength models.” Engng. Struct. 24(4):385–95.

650 Taljsten, B. (1996). “Strengthening of concrete prisms using the plate bonding technique.”
651 Int. J. Fract. 82(3): 253-66.
652 Wu, Y., Zhou, Z., Yang, Q., and Chen, W. (2010). “On shear bond strength of FRP-
653 concrete structures.” Eng. Struct. 32: 897-905.
654 Yang, Z.J., Chen, J.F., Proverbs, D. (2003). “Finite element modelling of concrete cover
655 separation failure in FEP plated RC beams.” Constr. Build. Mater. 17: 3-13.

656

657 **List of Figure Captions**

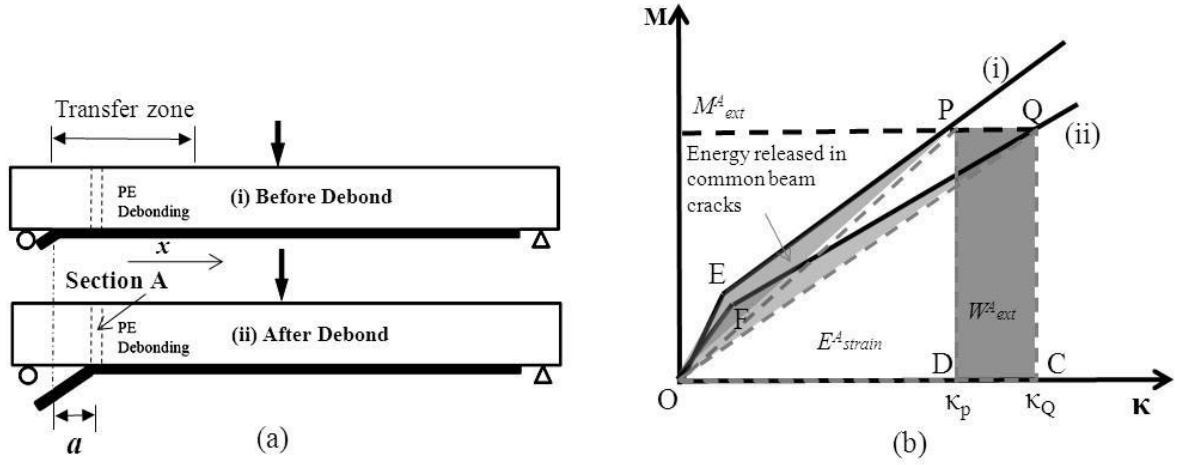

658

659 Figure 1 Comparison of the M-κ state of a section before and after debonding fracture
660 propagation

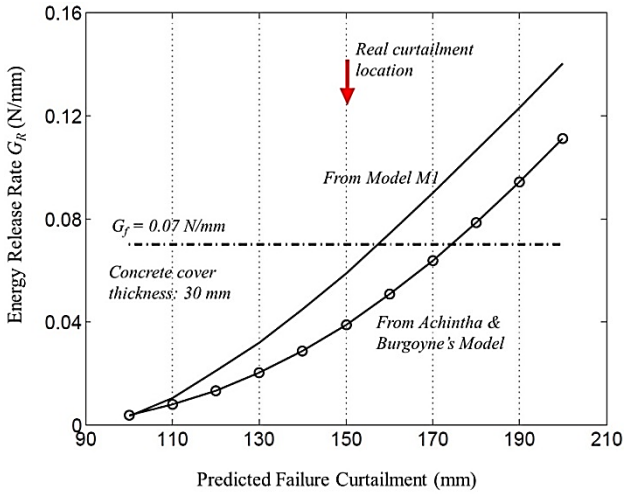

661

662 Figure 2 Comparison of a whole-section model M1 and Achintha & Burgoyne’s Model

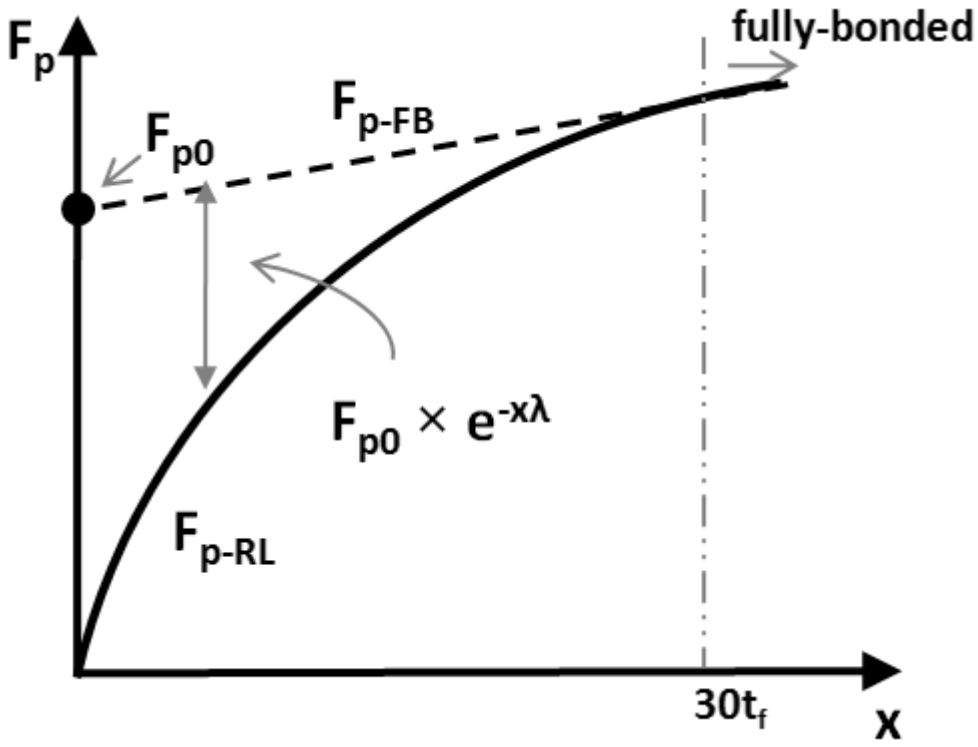

663

664 Figure 3 Relationship between the fully-bonded and the real FRP force

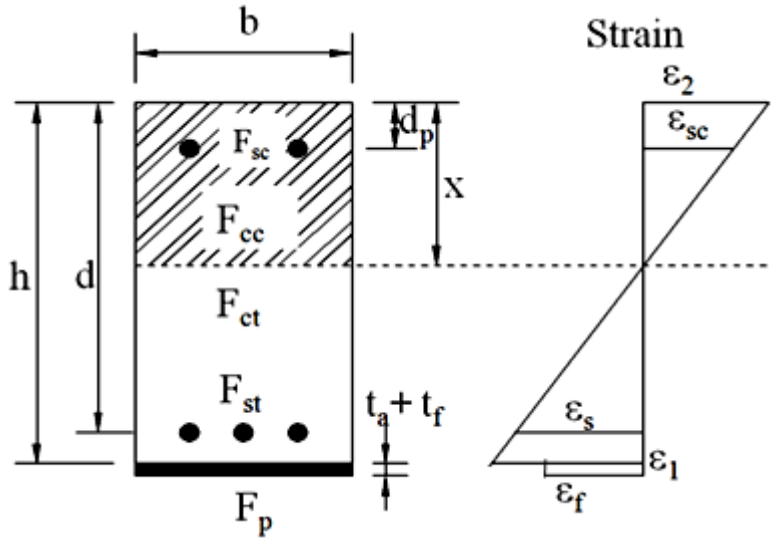

665

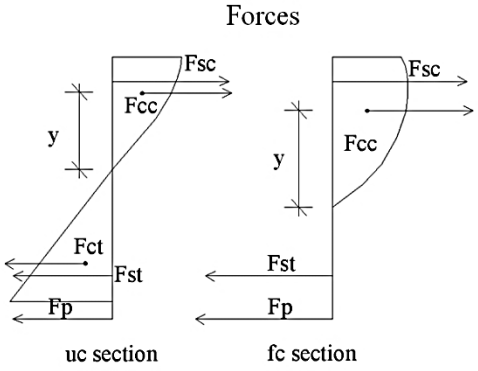

666

667 Figure 4 Section strain profile and forces (uc is uncracked; fc is fully-cracked)

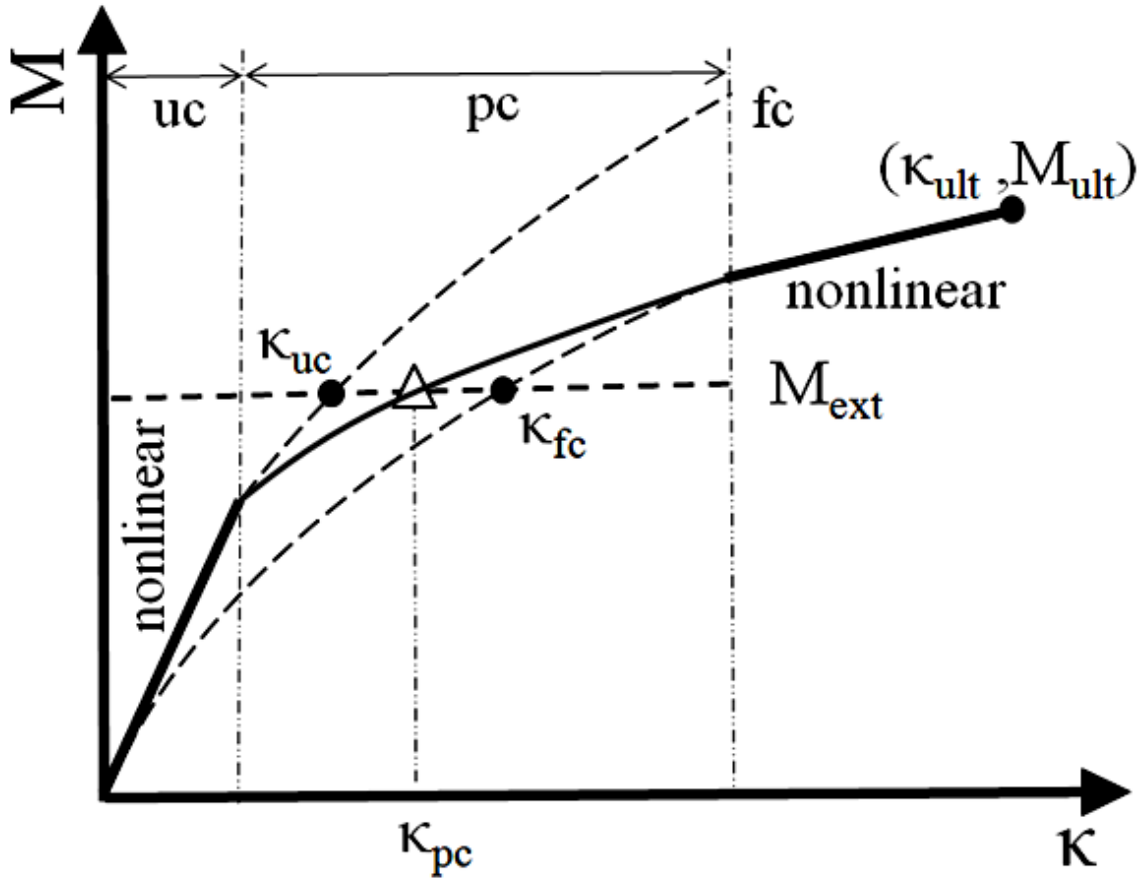

668

669 Figure 5 Conceptual formulation of the modified M-κ models

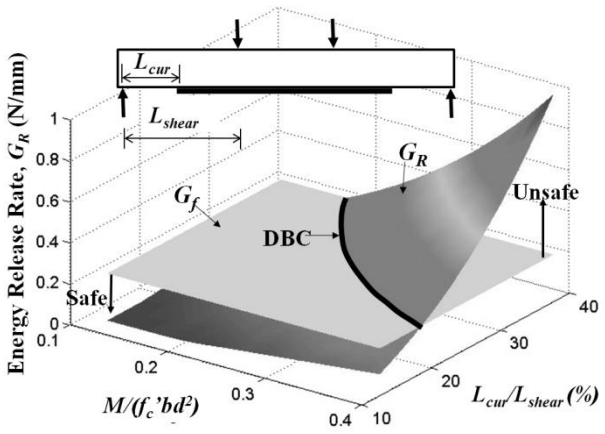

670

671 Figure 6 Fracture energy plane (G_f = 0.15 N/mm) and energy release rate (G_R) surfaces (For

672 a beam with h = 400 mm, $\rho_s = 1.0\%$, and $\rho_f = 0.5\%$)

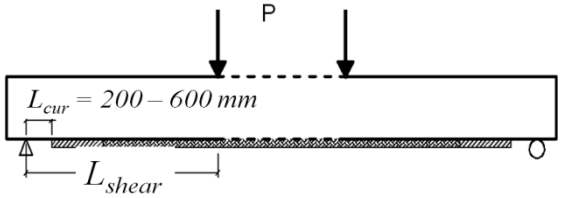

673

674 Figure 7 Dimensions of the standard beam

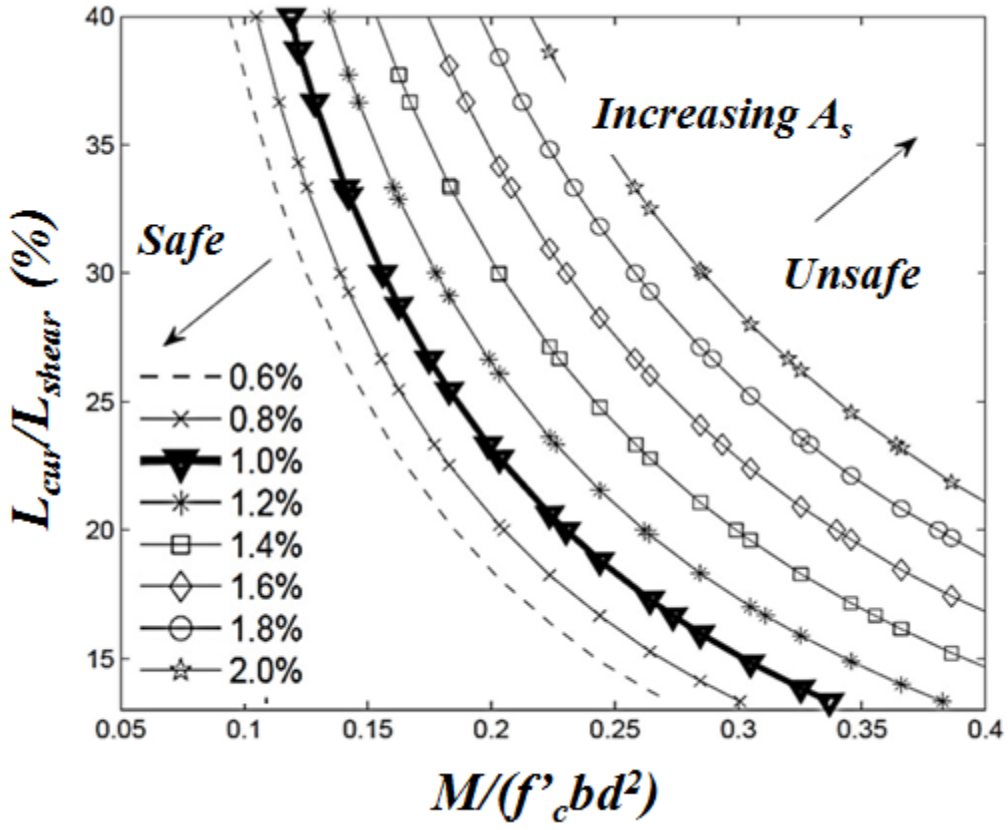

675

676 Figure 8 Effect of tension steel ratios (0.6-2.0%) on DBC with ρ_f = 0.5 %

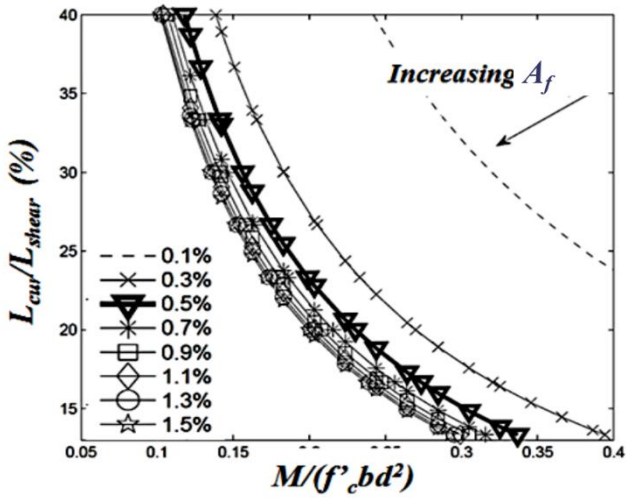

677

678 Figure 9 Effect of FRP ratios (0.1-1.5%) on DBC with ρ_s = 1.0 %

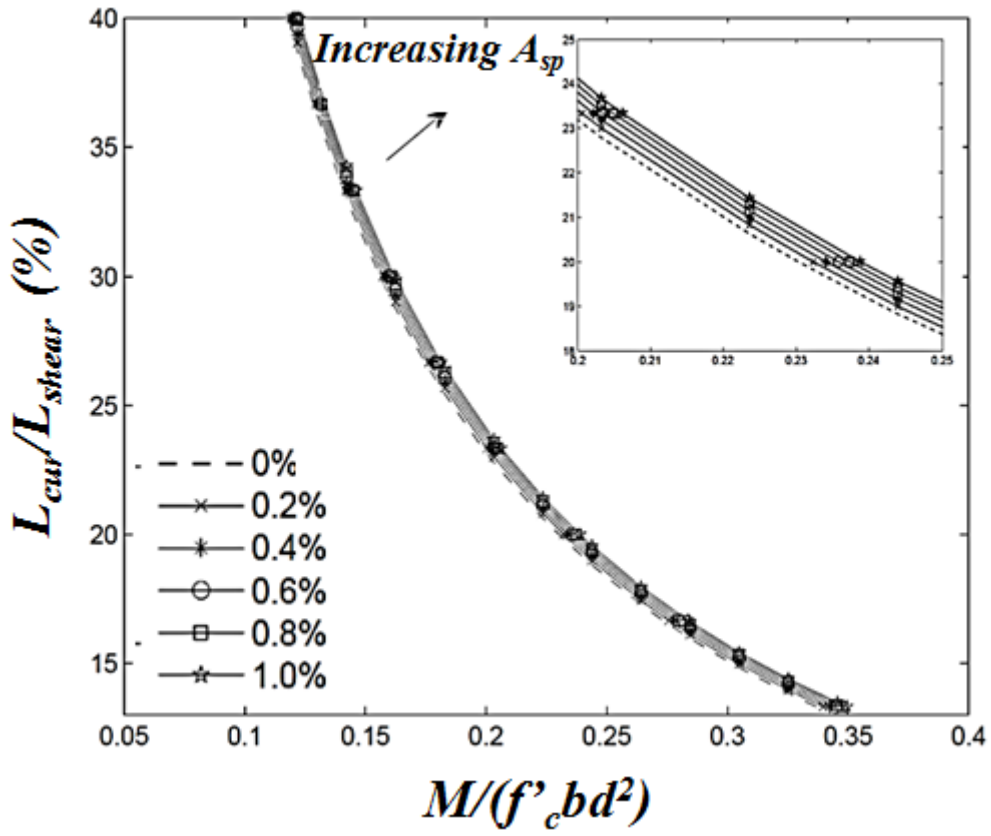

679

680 Figure 10 Effect of compression steel ratios (0-1.0%) on DBC (ρ_s = 1.0 % and ρ_f = 0.5 %)

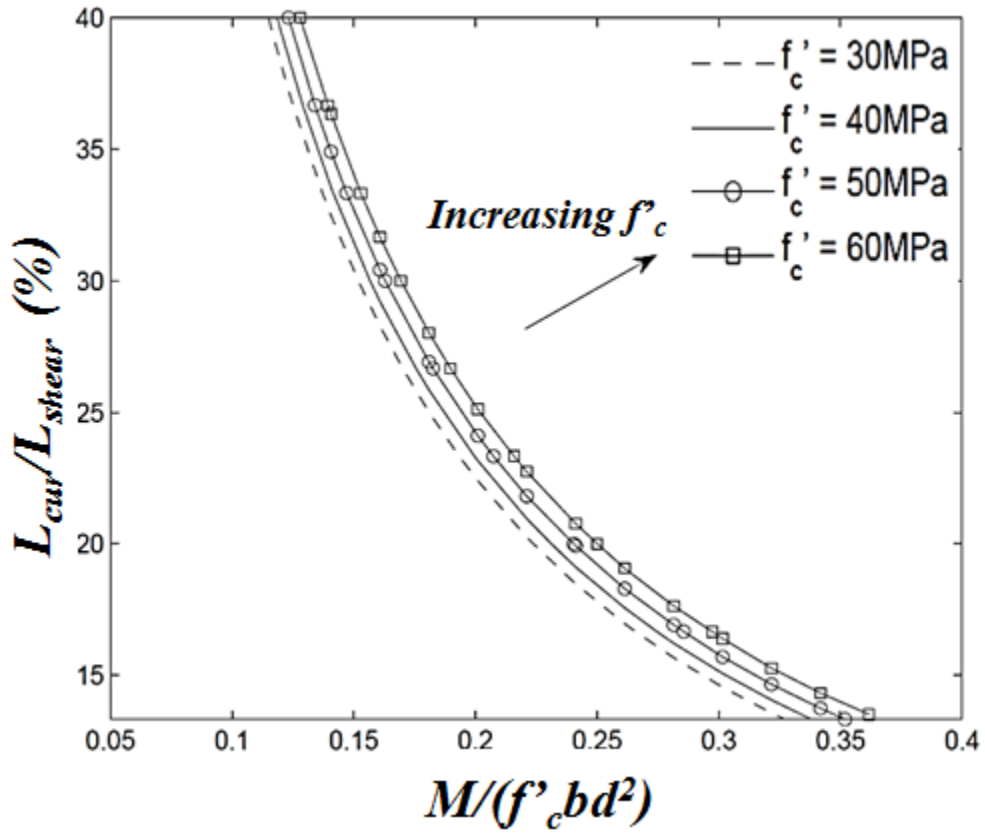

681

682 Figure 11 Effect of concrete compressive strength on DBC (ρ_s = 1.0 % and ρ_f = 0.5 %)

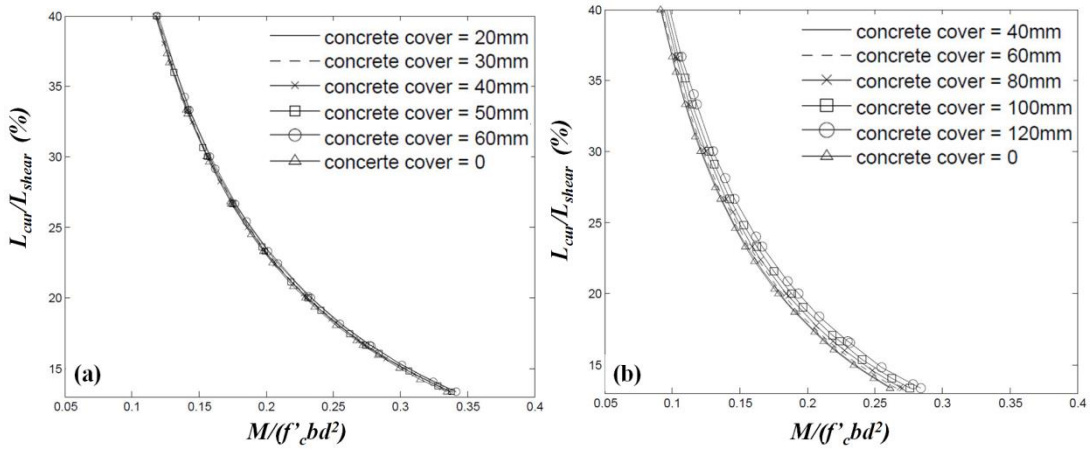

683

684 Figure 12 Effect of concrete cover thickness on DBC: (a) 400 mm Beam; (b) 800 mm Beam

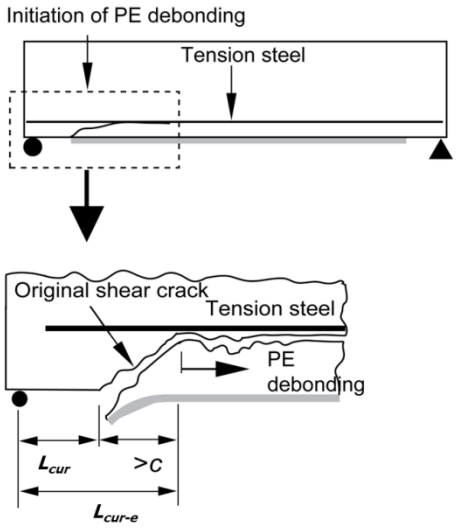

685

686 Figure 13 Location of the effective plate end (L_{cur-e})

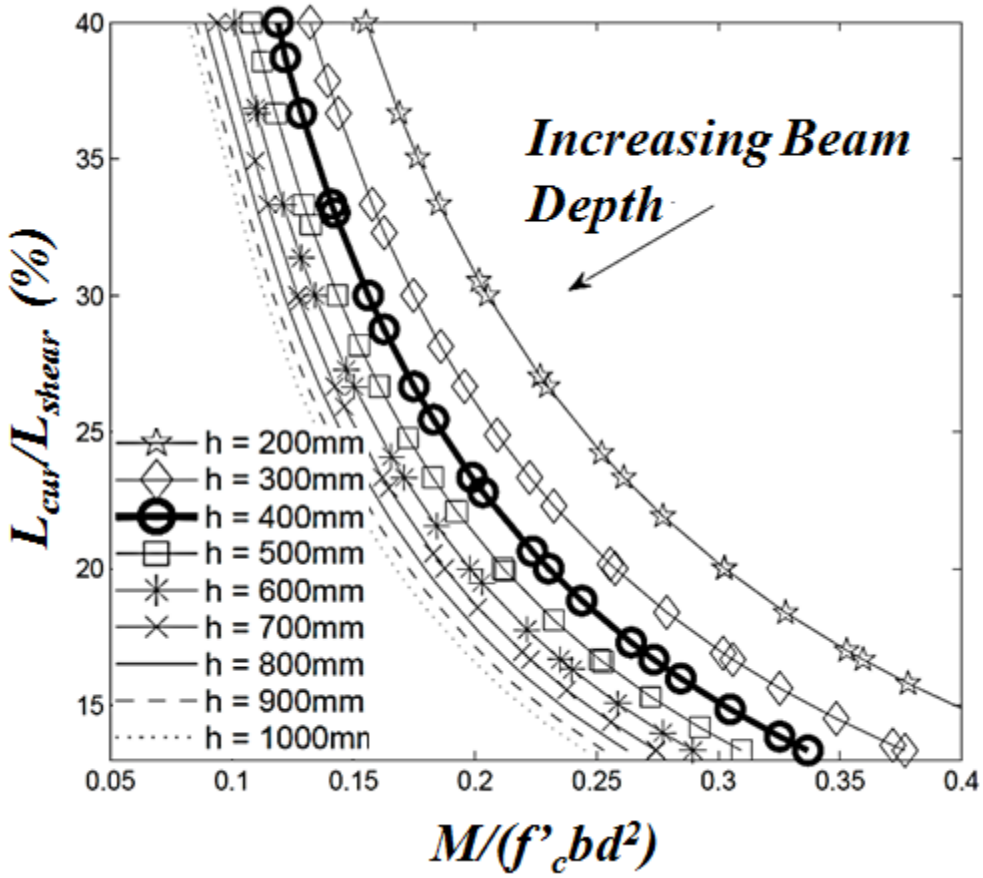

687

688 Figure 14 Effect of section depth on DBC of varying beam depth only. (L_{shear} is fixed at 1500

689 mm)

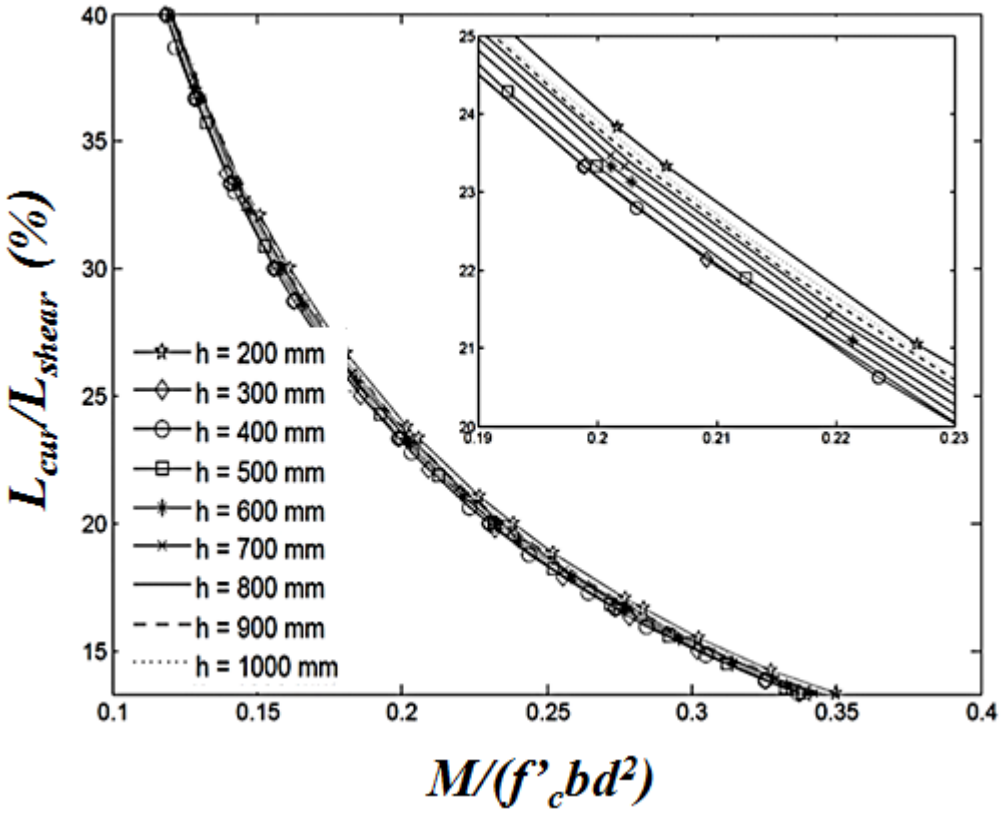

690

691 Figure 15 G_R contours for beams with different depths at $G_{f\text{-}q} = (G_f \times h)/400$

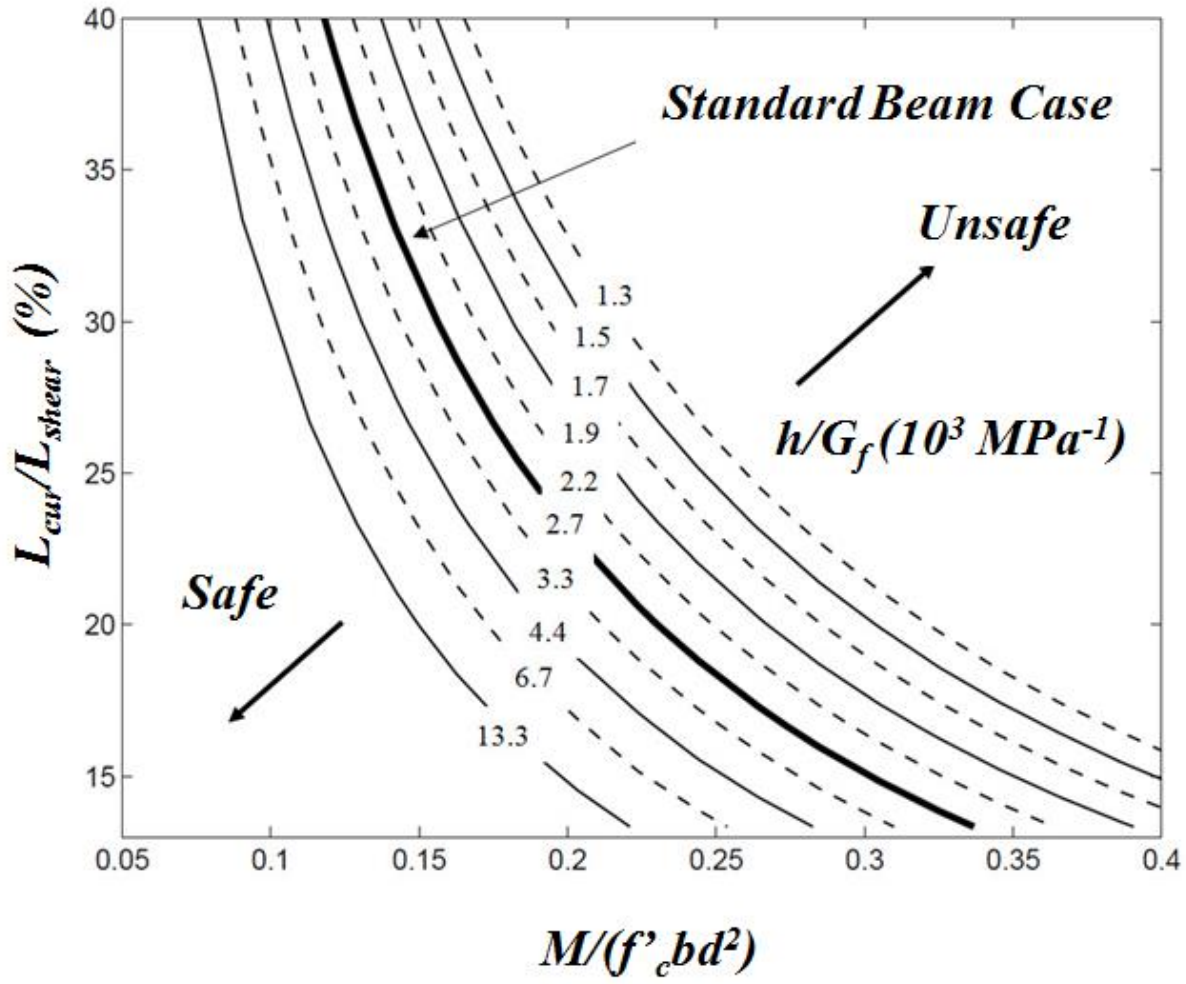

692

693 Figure 16 Normalized DBC for beams with different h/G_f values

694

695 Table 1 Properties of the Standard Beam

Depth (h)	400 mm	Steel Ratio ρ_s	1.0%
Concrete cover (c)	35 mm	FRP Ratio ρ_f	0.5%
Shear span (L_{shear})	1500 mm	Comp Steel Ratio ρ_{sp}	0
Steel yield strength f_y	530 MPa	Concrete strength f'_c	37 MPa
Nominal FRP thk	2 mm	FRP elastic modulus	165 GPa
Nominal Adhesive thk	1.5 mm	Adhesive elastic modulus	4.8 GPa

696

697